Metalloenzymes Hot Paper

How to cite: *Angew. Chem. Int. Ed.* **2023,** *62,* e202212224
International Edition: doi.org/10.1002/anie.202212224
German Edition: doi.org/10.1002/ange.202212224

Electrochemical Kinetics Support a Second Coordination Sphere Mechanism in Metal-Based Formate Dehydrogenase

*Marta Meneghello, Alexandre Uzel, Marianne Broc, Rita R. Manuel, Axel Magalon, Christophe Léger, Inês A. C. Pereira, Anne Walburger, and Vincent Fourmond**

Abstract: Metal-based formate dehydrogenases are molybdenum or tungsten-dependent enzymes that catalyze the interconversion between formate and CO_2. According to the current consensus, the metal ion of the catalytic center in its active form is coordinated by 6S (or 5S and 1Se) atoms, leaving no free coordination sites to which formate could bind to the metal. Some authors have proposed that one of the active site ligands decoordinates during turnover to allow formate binding. Another proposal is that the oxidation of formate takes place in the second coordination sphere of the metal. Here, we have used electrochemical steady-state kinetics to elucidate the order of the steps in the catalytic cycle of two formate dehydrogenases. Our results strongly support the "second coordination sphere" hypothesis.

Metal-based formate dehydrogenases (FDHs) are enzymes of the Mo/W-bis-PGD family[1] that catalyze the interconversion between formate and CO_2,[2] at an active site in which the metal (a W or Mo ion) is coordinated by two dithiolene ligands coming from two pyranopterin guanine dinucleotides (PGD), a cysteine or selenocysteine, and an inorganic sulfide.[3–5] Although it is now clear that the reaction catalyzed by FDHs is formally the abstraction of a hydride from formate to produce CO_2 (as opposed to the addition of an oxygen atom to produce bicarbonate),[6,7] the catalytic mechanism is still heavily debated. The main issue is that a sulfide ligand completes the coordination sphere of the metal to form a six S/Se coordination sphere, and that this ligand is required for activity.[3,5] As binding of a 7th ligand to an already saturated 6-S/Se coordination sphere seems unlikely, it is unclear how the substrate interacts with the active site.

A first series of putative mechanisms consider that the proteic ligand of the active site decoordinates so that the substrate can bind: Raaijmakers and Romao, based on a structure of *E. coli* FdhF in which the SeCys is uncoordinated, proposed that this decoordination step is part of the catalytic cycle.[8] A variation on this mechanism, proposed by Mota and co-workers using DFT computations,[9] suggests movement of the proteic ligand from the first to the second coordination sphere, via the formation of a S–Se or S–S bond, before complete decoordination in the course of catalysis. However, these mechanisms are not supported by the recent structural data obtained by some of us, which show that the SeCys ligand remains coordinated in all the redox states of the *Desulfovibrio vulgaris* Hildenborough FdhAB,[4,10] making it unlikely that decoordination is a requirement for catalysis. Another mechanism avoiding a 7-coordinated Mo/W was proposed by Niks and co-workers, who observed the formation of a 6-S Mo^V species coupled to a proton originating from formate upon exposure of FdsABG from *Cupriavidus necator* to formate. They concluded that formate does not directly bind to the active site metal, but rather stays in the second coordination sphere, and transfers a hydride to the molybdenum sulfide ligand.[11]

FDHs were first connected to electrodes by Reda and Hirst in 2008;[12] however, the number of articles describing FDHs directly wired to electrodes has only significantly increased in the past few years,[13] focusing either on mechanistic studies[7,14] or on the construction of biotechnological devices.[15] Here, we present kinetic data obtained using protein film electrochemistry with two FDHs, the recently characterized *Bacillus subtilis* (*Bs*) ForCE1[16] and *Desulfovibrio vulgaris* (*Dv*) FdhAB,[4] which allow us to clarify the sequence of the steps of formate binding and proton release during catalytic formate oxidation. Our data strongly support the "second coordination sphere" mechanism, without direct coordination of formate to the metal ion.

We immobilized *Bs* ForCE1 and *Dv* FdhAB onto pyrolytic graphite edge rotating-disc electrodes, in configurations that allow direct electron transfer. This makes it possible to measure the catalytic activity of the enzyme, recorded as an electrical current, as a function of various experimental parameters. This approach is called Protein

[*] M. Meneghello, A. Uzel, C. Léger, V. Fourmond
CNRS, Aix Marseille Université, BIP, IMM, IM2B
31 Chemin J. Aiguier, 13009 Marseille (France)
E-mail: vincent.fourmond@imm.cnrs.fr

A. Uzel, M. Broc, A. Magalon, A. Walburger
Aix Marseille Université, CNRS, Laboratoire de Chimie Bactérienne (UMR7283), IMM, IM2B
31 Chemin J. Aiguier, 13009 Marseille (France)

R. R. Manuel, I. A. C. Pereira
Instituto de Tecnologia Quimica e Biologica Antonio Xavier (ITQB NOVA), Universidade Nova de Lisboa
Oeiras (Portugal)

Film Electrochemistry.[17,18] Figure 1A shows a series of cyclic voltammograms (obtained by sweeping the electrode potential between two values and plotting the current as a function of potential) measured at various concentrations of formate with a film of *Bs* ForCE1. The electrode was spun at a high rate to prevent substrate depletion. The current traces of the forward and backward scans are just offset by the capacitive current of the electrode (dashed black curve in Figure 1A), showing that the catalytic response is under steady-state. Figure 1B shows the baseline-subtracted voltammograms. The shape of each response is simple, with a sigmoidal increase in an intermediate potential range, and the linear increase at high potential that reveals a distribution of enzyme orientation.[19,20] Upon increasing the concentration of formate, the amplitude of the signal increases and its position shifts to lower potentials.

To quantitatively characterize the effect of the concentration of formate, we fitted a simple model[21] to the baseline-subtracted voltammograms. In this model, we assume that the enzyme active site cycles between three redox states (IV, V and VI), and that the substrate-bound VI state reacts in an irreversible manner to produce the IV state and release the product. The model reproduces the data with excellent accuracy (gray dashed lines in Figure 1B). Figure 1C shows that the same model can also be satisfactorily fitted to the data obtained with *Dv* FdhAB (see Supporting Information Figure S1 for a plot including the raw data obtained with *Dv* FdhAB and the residuals for both enzymes).

Each fit returns 5 parameters: two reduction potentials: $E_{6/5}$ (the potential of the VI to V redox couple) and $E_{5/4}$ (V to IV), the corresponding rates of electron transfer ($k_0^{6/5}$ and $k_0^{5/4}$, not discussed here), and a $i_{lim}/\beta d_0$ parameter that is proportional to the limiting current, therefore to the catalytic rate at infinite driving force.[19,21] Next, we analyzed how these parameters change as a function of the experimental conditions (formate concentration and pH) to determine how substrate binding and deprotonation events are coupled to electron transfer steps.

We first considered the influence of formate concentration on the fit parameters. Figure 2 shows the variation of the redox potentials (panel A) and of the current (blue circles in panel C) as a function of substrate concentration obtained from the *Bs* ForCE1 data shown in Figure 1B. Figure 2A shows that the V/IV potential ($E_{5/4}$, red circles) decreases by 60 mV per decade of substrate concentration at high substrate concentration, indicating that the oxidation from IV to V is coupled to substrate binding. The VI/V potential ($E_{6/5}$, green squares) is independent of substrate concentration, which indicates that the energetics of the V to VI oxidation are independent of the presence of

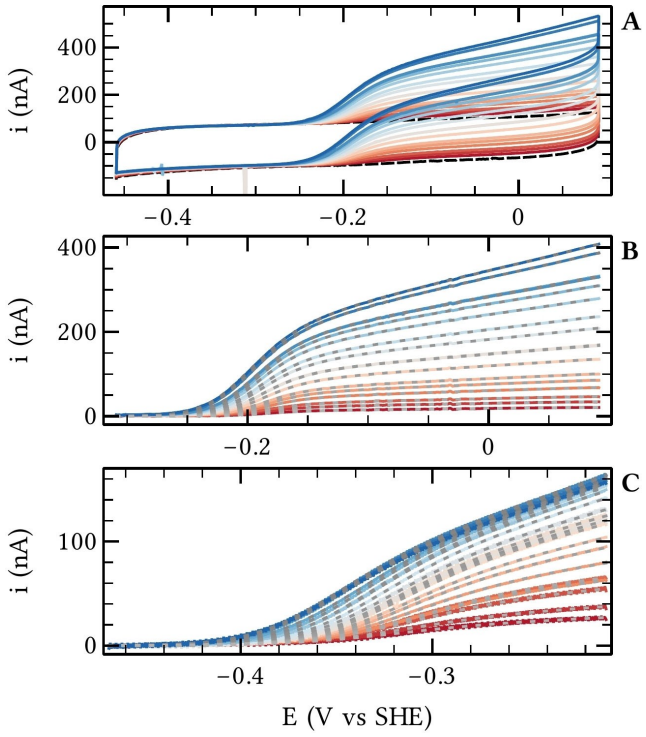

Figure 1. Cyclic voltammograms of films of (A– B) *Bs* ForCE1 and (C) *Dv* FdhAB, with increasing concentrations of formate (from red to blue). A) Raw voltammograms (the black dashed curve is the blank). B) and C) Baseline-subtracted data (solid colored lines), together with their fits (gray dotted lines, see text). Conditions: 20 mV s^{-1}, pH 7, T = (A–B) 40 °C, (C) 25 °C. See full conditions in Supporting Information. The raw data for *Dv* FdhAB and the residuals are shown in supplementary Figure S1.

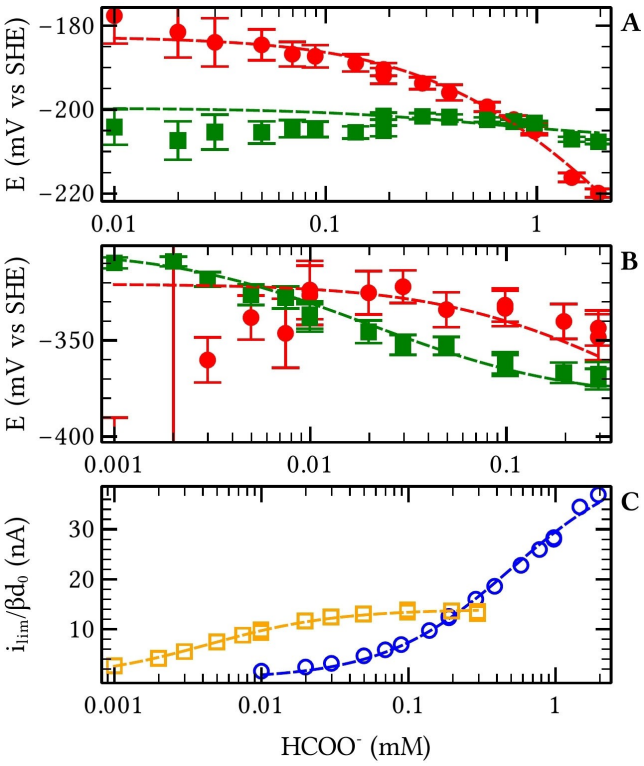

Figure 2. Parameters of the fits to the data shown in Figure 1. In panels A (*Bs* ForCE1) and B (*Dv* FdhAB) the red circles correspond to $E_{5/4}$, the green squares to $E_{6/5}$. Panel C shows the values of $i_{lim}/\beta d_0$ for ForCE1 (blue circles) and FdhAB (orange squares). The dashed lines are the fits of Equations (1), (2) and (3) to the data. The error bars correspond to the 95% confidence intervals of the fits of Figure 1.

substrate, so that the energetics of binding are identical for the V or VI states. In summary, formate binds with equal affinity to the two most oxidized states of the active site (V and VI) [cf. Eq. (2) below], but not to Mo^{IV} [Eq. (1)], resulting in the catalytic cycle depicted in scheme 1.

Scheme 1 predicts the following relations between the potentials of the V/IV and of the VI/V couples ($E_{5/4}$ and $E_{6/5}$), the potentials of the substrate-free V/IV and VI/V couples ($E_{5/4}^{free}$ and $E_{6/5}^{free}$) and the binding constants of the substrate to the V and VI states (K_5 and K_6)[22] (see full derivation in Supporting Information):

$$E_{5/4} = E_{5/4}^{\mathrm{free}} - \frac{RT}{F}\ln\left(1+\frac{[S]}{K_5}\right) \quad (1)$$

$$E_{6/5} = E_{6/5}^{\mathrm{free}} + \frac{RT}{F}\ln\frac{1+[S]/K_5}{1+[S]/K_6} \quad (2)$$

where [S] is the substrate concentration (the $E_{6/5}^{bound}$ potential of the substrate-bound active site is not a parameter of the fit since its value can be deduced from the other parameters using thermodynamic constraints). The limiting current is given by:

$$i_{\mathrm{lim}}/\beta d_0 = i_{\mathrm{lim}}^{\mathrm{max}}/\beta d_0 \times \frac{1}{1+K_6/[S]} \quad (3)$$

where $i_{lim}^{max}/\beta d_0$ is the value of $i_{lim}/\beta d_0$ under saturating conditions. The Michaelis constant at infinite driving force is therefore the equilibrium constant for binding to the VI state of the active site (K_6).

By fitting these equations to the data in Figure 2, we determined the binding constants and the potentials of the active site transitions without substrate. In the case of *Bs* ForCE1, the results of the fit confirm that the equilibrium constants for substrate binding to the active site are similar for both the V and the VI states: $K_5 = 0.66$ mM and $K_6 = 0.5$ mM for the data shown in Figure 2. The value of K_6 is consistent with the published value of K_m of 5 mM determined under different conditions (pH 10, $T = 25\,^{\circ}C$[16]).

This model can also be successfully fitted to the data obtained by analyzing the *Dv* FdhAB voltammograms (Figure 1C), shown in Figure 2 (panel B and orange squares in panel C). The main difference with ForCE1 is the existence of a range of concentration in which the potential of the VI/V couple decreases slightly, reflecting weaker binding to the V state than to the VI state. Fitting Equations (1)–(3) to the data in Figure 2 gives $K_5 = 90$ μM and $K_6 = 5$ μM. These values are also consistent with the published values of K_m of 17 μM at pH 7.6.[4] The deviation between the model and the fitted values of $E_{5/4}$ (red circles in Figure 2) at low formate concentrations arise from the fact that they are much less accurately determined than the values of $E_{6/5}$, and hence they were given less weight in the fit of Equations (1)–(3) to the six data sets in Figure 2.

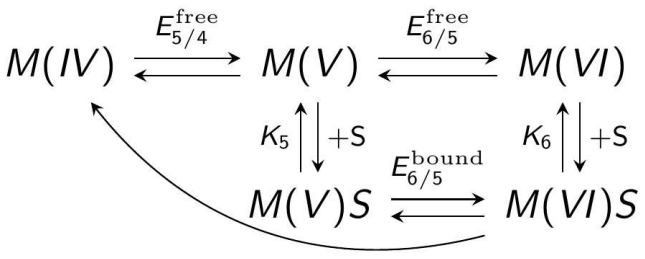

Scheme 1. Kinetic scheme used for modeling the dependence of the potentials on substrate concentration. M is either Mo or W depending on the enzyme.

To learn about proton transfers, we repeated experiments such as those shown in Figure 1 with the two enzymes at different pH values, and we repeated the analysis described in Figure 2 for each of those. The results are shown in Figure 3. The parameters obtained for each pH are the two potentials of the free enzyme, and the two equilibrium constants for the binding of formate to the two most oxidized states. In the case of *Bs* ForCE1, the two equilibrium constants have the same magnitude and hardly change with pH (Figure 3C). $E_{6/5}^{free}$ is independent of pH, whereas the dependence of $E_{5/4}^{free}$ is −60 mV/pH (Figure 3A). Together with the data in Figure 2A, this demonstrates that the Mo^{IV} to Mo^{V} oxidation step is coupled to a deprotonation and to formate binding.

The determination of the *Dv* FdhAB potentials is less accurate (because the signal was smaller, and baseline correction harder), but the pH dependences of $E_{5/4}^{free}$ and $E_{6/5}^{free}$ shown in Figure 3B (−30 mV/pH in average) are consistent with the two-electron oxidation of W^{IV} being coupled to the abstraction of a single proton (as in *Bs* ForCE1). The two pH dependencies are best explained by assuming a pK_a of 6.5 for the W^{V} state (the dashed lines in Figure 3B are calculated under this assumption). For both enzymes, deprotonation and substrate binding occur in the same step. In the case of *Bs* ForCE1, they occur when Mo^{IV} is oxidized to Mo^{V}, whereas in the case of *Dv* FdhAB, they are coupled to either the W^{IV}-to-W^{V} or the W^{V}-to-W^{VI} oxidation, depending on pH. Note that the data of Figure 3B are consistent with the results of a recent EPR titration of *Dv* FdhAB.[10]

The data we obtained by modeling the dependence of the catalytic wave shape on formate concentration and pH strongly constrain the possible mechanisms of catalytic formate oxidation. We observed that the two-electron oxidation of the active site is coupled to one deprotonation (as expected from the stoichiometry of the overall catalytic reaction), which occurs in the (IV) to (V) step independently of pH in the case of *Bs* ForCE1, and in one redox step or the other depending on pH in the case of *Dv* FdhAB. In its fully reduced state (IV), the active site does not bind formate in the concentration range we studied, but formate binding and deprotonation are coupled to the same redox step. Therefore, substrate binding is dependent on the deprotonation of the active site. Furthermore, formate binds to the (V) or (VI) states with about the same affinity, which argues against the hypothesis that formate directly coordinates the metal. Similar or even complementary information

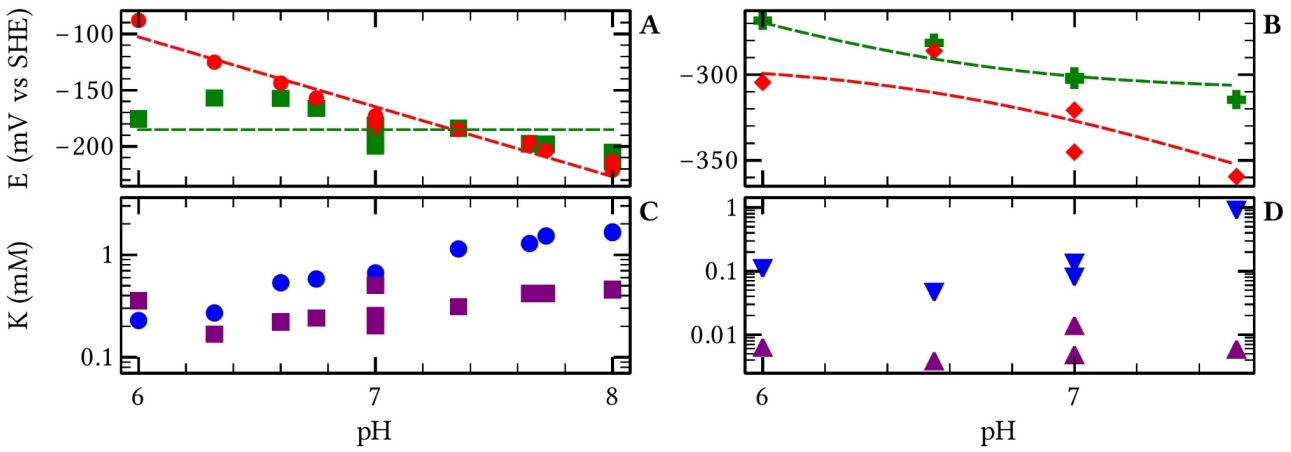

Figure 3. Results of the fits of a series of voltammograms recorded at different pHs for (A, C) *Bs* ForCE1 and (B, D) *Dv* FdhAB . A) and B) Potentials of the substrate-free enzyme: $E_{5/4}^{free}$ (red circles) and $E_{6/5}^{free}$ (green squares). The red line in panel A corresponds to a $1\,H^+/1\,e^-$ coupled transfer. The curves in panel B correspond to the prediction of a $1\,H^+/2\,e^-$ scheme[23] with a pK_a of 6.5 for the W^V state. C) and D) Binding constants: K_5 in blue, K_6 in purple. Duplicate points at pH 7 correspond to distinct experiments.

could probably be obtained by monitoring the CO_2 reduction current. However, we focused here on formate oxidation since it is far harder to change the concentrations of dissolved CO_2 than formate, and the CO_2 reduction currents we observed are smaller than those of formate oxidation.

It is remarkable that the potentials of the active site of *Bs* ForCE1 are significantly above those of *Dv* FdhAB, consistent with the shift of the waves towards low potentials for FdhAB visible in Figure 1. The high potentials of the VI/V transition is consistent with values of about −160 mV found for the Mo FDH from *Desulfovibrio desulfuricans*.[24] The increase in potential for the Mo enzymes is reminiscent of the observations that substituting Mo by W in the case of the DMSO reductase led to a decrease of about 200 mV in the reduction potentials of the active site[25].

Our observations support a slight modification of the "second coordination sphere catalysis" mechanism proposed by Niks and co-workers[11] that is shown in Figure 4. For *Bs* ForCE1, upon starting the cycle from the $Mo^{VI}S$ state, formate is in the active site pocket with its single proton close to the catalytic sulfide. Then, the concerted transfer of the proton to the sulfide and of two electrons to the metal center produces a CO_2 molecule, which diffuses away, and brings the active site in a protonated Mo^{IV} state. Formate cannot productively approach the active site in this state as long as the proton is bound to the sulfide ligand. Oxidation to Mo^V, coupled to deprotonation, allows formate to bind in a configuration in which proton transfer to the sulfide is possible. Catalysis proceeds with formate binding and another one-electron oxidation, which may occur in any order (formate binding first or oxidation first).

This mechanism also applies to *Dv* FdhAB (replacing Mo by W), with one small modification: the pK_a of the W^V species is high enough that deprotonation is not necessarily coupled to oxidation to W^V, but, depending on pH, can also occur only during the oxidation to W^{VI}. Only then can the substrate bind. This observation is compatible with the observation by Niks et al. of a formate-derived proton coupled to a Mo^V signal[11] in the case of *Cupriavidus necator* FdsAB. It is also in line with the lower affinity of the W^V state for the substrate, and suggests that substrate binding may shift the deprotonation equilibrium.

In recent years, various data have been published in favor of the "second coordination sphere" mechanism, such as evidence for the lack of decoordination in all redox states of *Dv* FdhAB,[4,10] the formation of a 6-S Mo^V species coupled to a formate-derived proton after exposure of *Cupriavidus necator* FdsAB, but also a number of theoretical works suggesting that direct binding of formate to Mo is prohibitively endergonic.[26,27] Robinson and co-workers proposed that the decoordination of the SeCys corresponds to a reductive activation step observed in electrochemistry;[14] however, the closely related periplasmic nitrate reductase also undergoes a reductive activation[28] that was shown to arise from a change in the pterin cofactor rather than a change in metal coordination.[29] Other evidences of decoordination were obtained with *Rhodobacter capsulatus* FDH. The cysteine ligand to Mo was shown to be alkylated, but only in the presence of nitrate.[30] It was further shown by X-ray absorption spectroscopy to change active site ligands upon exposure to formate.[31] However, recent IR data show that the competitive inhibitor azide binds to the second coordination sphere,[32] which is compatible with the mechanistic proposal of Figure 4. Here, the observation that the binding constants for formate from the (V) and (VI) states are almost identical is a strong argument against the direct coordination of formate to the metal.

The mechanism shown in Figure 4 is strikingly reminiscent of that of metal-free formate dehydrogenases, which transfer a hydride from formate to NAD^+.[33] However, it is not appropriate to think of the Mo/W active site as a "substitute" for NAD^+: as emphasized by Yang and co-workers, the FDH reaction is not a hydride transfer, but rather the concomitant transfer of a proton and two

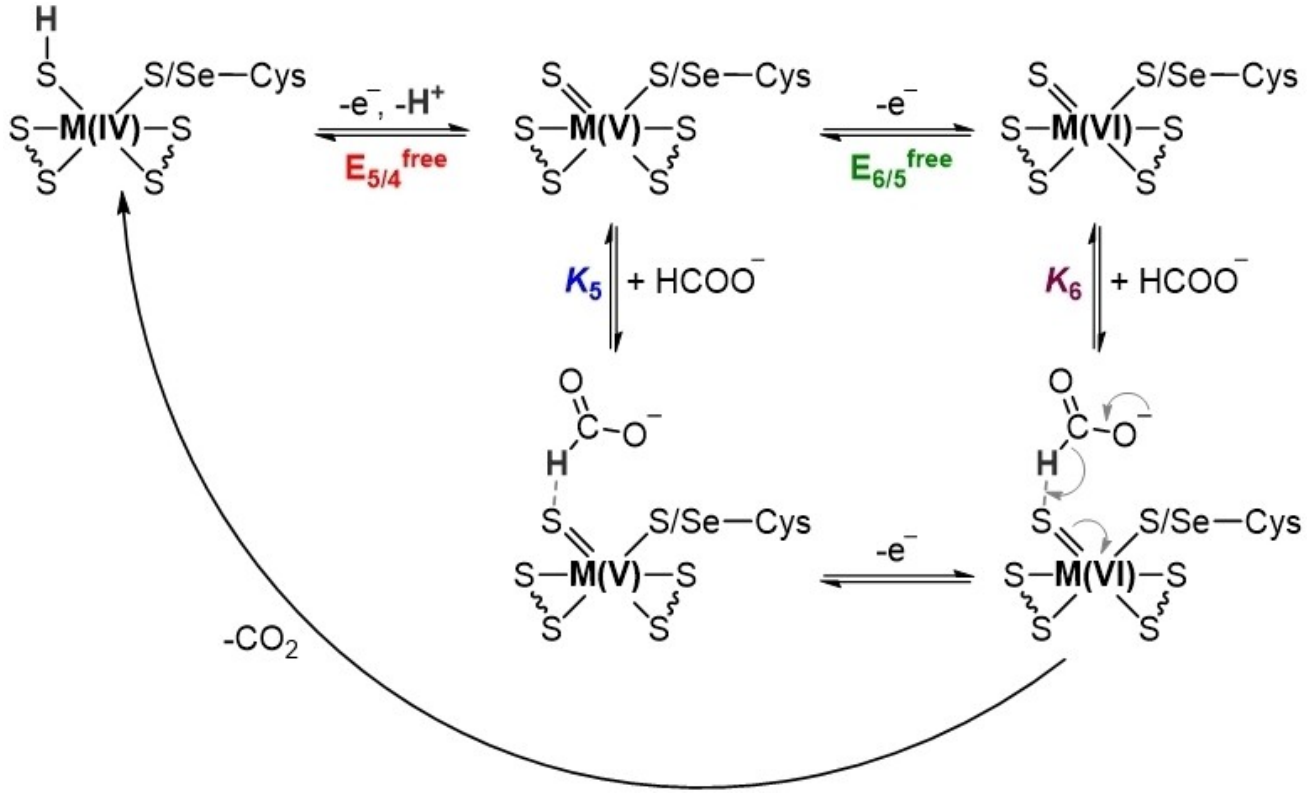

Figure 4. Proposed catalytic mechanism. M can either be Mo or W.

electrons, with two different targets.[34] This separation is necessary because metal hydrides with sufficient hydricity to reduce CO_2 can unfortunately only be reduced at potentials incompatible with the catalytic reversibility[35] of FDH.

Supporting Information

Procedures for protein purification, experimental conditions, derivations of Equations (1)–(3) and Supporting Information Figure S1.

Acknowledgements

The authors acknowledge support from CNRS, Agence Nationale de la Recherche (grants ANR-14-CE05-0010, ANR-15-CE05-0020, ANR-17-CE11-0027, ANR-18-CE05-0029), and Region PACA, . The project leading to this publication has received funding from Excellence Initiative of Aix-Marseille University—A*Midex, a French "Investissements d'Avenir" program. M.M., C.L., and V.F. are members of the French Bioinorganic Chemistry group (http://frenchbic.cnrs.fr). We also acknowledge support from Fundação para a Ciência e Tecnologia (grant PTDC/BII-BBF/2050/2020 and fellowship DFA/BD/7897/2020), MOSTMICRO-ITQB unit (UIDB/04612/2020 and UIDP/04612/2020) and Associated Laboratory LS4FUTURE (LA/P/0087/2020), and support from the MOSBRI project, which has received funding from the European Union's Horizon 2020 Research and Innovation Programme under Grant Agreement N° 101004806.

Conflict of Interest

The authors declare no conflict of interest.

Data Availability Statement

The data that support the findings of this study are available from the corresponding author upon reasonable request.

Keywords: Metalloenzymes · Enzyme catalysis · Electrochemistry · Mo/W formate dehydrogenase · Second coordination sphere

[1] S. Grimaldi, B. Schoepp-Cothenet, P. Ceccaldi, B. Guigliarelli, A. Magalon, *Biochim. Biophys. Acta Bioenerg.* **2013**, *1827*, 1048–1085.
[2] L. B. Maia, J. J. G. Moura, I. Moura, *J. Biol. Inorg. Chem.* **2015**, *20*, 287–309.
[3] R. Thomé, A. Gust, R. Toci, R. Mendel, F. Bittner, A. Magalon, A. Walburger, *J. Biol. Chem.* **2012**, *287*, 4671–4678.
[4] A. R. Oliveira, C. Mota, C. Mourato, R. M. Domingos, M. F. A. Santos, D. Gesto, B. Guigliarelli, T. Santos-Silva,

M. J. Romão, I. A. Cardoso Pereira, *ACS Catal.* **2020**, *10*, 3844–3856.
[5] P. Schrapers, T. Hartmann, R. Kositzki, H. Dau, S. Reschke, C. Schulzke, S. Leimkühler, M. Haumann, *Inorg. Chem.* **2015**, *54*, 3260–3271.
[6] S. V. Khangulov, V. N. Gladyshev, G. C. Dismukes, T. C. Stadtman, *Biochemistry* **1998**, *37*, 3518–3528.
[7] M. Meneghello, A. R. Oliveira, A. Jacq-Bailly, I. A. C. Pereira, C. Léger, V. Fourmond, *Angew. Chem. Int. Ed.* **2021**, *60*, 9964–9967; *Angew. Chem.* **2021**, *133*, 10052–10055.
[8] H. C. A. Raaijmakers, M. J. Romão, *J. Biol. Inorg. Chem.* **2006**, *11*, 849–854.
[9] C. S. Mota, M. G. Rivas, C. D. Brondino, I. Moura, J. J. G. Moura, P. J. González, N. M. F. S. A. Cerqueira, *J. Biol. Inorg. Chem.* **2011**, *16*, 1255–1268.
[10] A. R. Oliveira, C. Mota, K. Klymanska, F. Biaso, M. J. Romão, B. Guigliarelli, I. C. Pereira, *ACS Chem. Biol.* **2022**, *17*, 1901–1909.
[11] D. Niks, J. Duvvuru, M. Escalona, R. Hille, *J. Biol. Chem.* **2016**, *291*, 1162–1174.
[12] T. Reda, C. M. Plugge, N. J. Abram, J. Hirst, *Proc. Natl. Acad. Sci. USA* **2008**, *105*, 10654–10658.
[13] M. Meneghello, C. Léger, V. Fourmond, *Chem. Eur. J.* **2021**, *27*, 17542–17553.
[14] W. E. Robinson, A. Bassegoda, E. Reisner, J. Hirst, *J. Am. Chem. Soc.* **2017**, *139*, 9927–9936.
[15] M. Miller, W. E. Robinson, A. R. Oliveira, N. Heidary, N. Kornienko, J. Warnan, I. A. C. Pereira, E. Reisner, *Angew. Chem. Int. Ed.* **2019**, *58*, 4601–4605; *Angew. Chem.* **2019**, *131*, 4649–4653.
[16] R. Arias-Cartín, A. Uzel, F. Seduk, G. Gerbaud, F. Pierrel, M. Broc, R. Lebrun, B. Guigliarelli, A. Magalon, S. Grimaldi, A. Walburger, *J. Biol. Chem.* **2022**, *298*, 101384.
[17] C. Léger, P. Bertrand, *Chem. Rev.* **2008**, *108*, 2379–2438.
[18] M. Del Barrio, M. Sensi, C. Orain, C. Baffert, S. Dementin, V. Fourmond, C. Léger, *Acc. Chem. Res.* **2018**, *51*, 769–777.
[19] C. Léger, A. K. Jones, S. P. J. Albracht, F. A. Armstrong, *J. Phys. Chem. B* **2002**, *106*, 13058–13063.
[20] V. Fourmond, C. Baffert, K. Sybirna, T. Lautier, A. Abou Hamdan, S. Dementin, P. Soucaille, I. Meynial-Salles, H. Bottin, C. Léger, *J. Am. Chem. Soc.* **2013**, *135*, 3926–3938.
[21] V. Fourmond, C. Léger, *Curr. Opin. Electrochem.* **2017**, *1*, 110–120.
[22] C. Léger, K. Heffron, H. R. Pershad, E. Maklashina, C. Luna-Chavez, G. Cecchini, B. A. Ackrell, F. A. Armstrong, *Biochemistry* **2001**, *40*, 11234–11245.
[23] E. Laviron, *J. Electroanal. Chem. Interfacial Electrochem.* **1983**, *146*, 1–13.
[24] C. Costa, M. Teixeira, J. LeGall, J. J. G. Moura, I. Moura, *J. Biol. Inorg. Chem.* **1997**, *2*, 198–208.
[25] P. L. Hagedoorn, W. R. Hagen, L. J. Stewart, A. Docrat, S. Bailey, C. D. Garner, *FEBS Lett.* **2003**, *555*, 606–610.
[26] G. Dong, U. Ryde, *J. Biol. Inorg. Chem.* **2018**, *23*, 1243–1254.
[27] P. E. M. Siegbahn, *J. Phys. Chem. B* **2022**, *126*, 1728–1733.
[28] V. Fourmond, B. Burlat, S. Dementin, P. Arnoux, M. Sabaty, S. Boiry, B. Guigliarelli, P. Bertrand, D. Pignol, C. Léger, *J. Phys. Chem. B* **2008**, *112*, 15478–15486.
[29] J. G. J. Jacques, V. Fourmond, P. Arnoux, M. Sabaty, E. Etienne, S. Grosse, F. Biaso, P. Bertrand, D. Pignol, C. Léger, B. Guigliarelli, B. Burlat, *Biochim. Biophys. Acta Bioenerg.* **2014**, *1837*, 277–286.
[30] T. Hartmann, P. Schrapers, T. Utesch, M. Nimtz, Y. Rippers, H. Dau, M. A. Mroginski, M. Haumann, S. Leimkühler, *Biochemistry* **2016**, *55*, 2381–2389.
[31] B. R. Duffus, P. Schrapers, N. Schuth, S. Mebs, H. Dau, S. Leimkühler, M. Haumann, *Inorg. Chem.* **2020**, *59*, 214–225.
[32] K. Laun, B. Duffus, S. M. Wahlefeld, S. Katz, D. Belger, P. Hildebrandt, M. A. Mroginski, S. Leimkühler, I. Zebger, *Chem. Eur. J.* **2022**, *28*, e202201091.
[33] V. O. Popov, V. S. Lamzin, *Biochem. J.* **1994**, *301(Pt3)*, 625–643.
[34] J. Y. Yang, T. A. Kerr, X. S. Wang, J. M. Barlow, *J. Am. Chem. Soc.* **2020**, *142*, 19438–19445.
[35] V. Fourmond, N. Plumeré, C. Léger, *Nat. Chem. Rev.* **2021**, *5*, 348–360.

Manuscript received: August 18, 2022
Accepted manuscript online: December 5, 2022
Version of record online: January 3, 2023